Solid Freeform Fabrication 2021: Proceedings of the 32nd Annual International
Solid Freeform Fabrication Symposium – An Additive Manufacturing Conference
Reviewed Paper

PROCESSABILITY OF SODA-LIME GLASS IN LASER-BASED POWDER BED FUSION

C. Singer[a], S. Platt[b], M. Horn[a], M. Binder[a], M. Piechotta[b], J. Wegner[b], S. Kleszczynski[b] and C. Seidel[a,c], G. Witt[b], J. Schilp[a,d]

[a]Fraunhofer Institute for Casting, Composite and Processing Technology IGCV, 86159 Augsburg, Germany

[b]University of Duisburg-Essen, Institute of Product Engineering, Manufacturing Technology, 47057 Duisburg, Germany

[c]University of Applied Sciences Munich, Department for Mechatronics and Applied Sciences, Munich 80335, Germany

[d]University of Augsburg, Chair of Digital Manufacturing, Department of Applied Computer Science, 86159 Augsburg, Germany

Abstract

Processing of electrically insulating materials with high temperature resistance is a major challenge in laser-based powder bed fusion (PBF-LB). Glasses form a promising material class, which also offers the potential for manufacturing optical or electronic components while having high chemical resistance. Therefore, this paper investigates the processability of soda-lime glass in conventional PBF-LB machines using Yb:YAG and CO_2 lasers. Firstly, the flow properties and particle shape of the glass powder were inspected. Secondly, the influence of laser power, scan velocity, layer height and hatch distance as well as exposure pattern on the manufacturing of single tracks, single layers, and finally 3-D-parts was investigated. Furthermore, an increase of the temperature of the platform range between 250 to 600 °C resulted in increasing relative density. Despite the higher absorptivity of soda lime glass in the wavelength range of the CO_2 laser, manufacturing of 3-D-parts was only possible using a Yb:YAG laser due to insufficient laser power of the former beam source.

Introduction

Glass materials are a beneficial choice for many different applications ranging from the medical and chemical industries to the manufacturing of electronics but also architectural industry. Their chemical resistance, transparency, thermal stability as well as high electrical resistivity allow the use for a wide range of applications like optical components, insulators, or design objects.

In multi-material additive manufacturing or automated integration of sensors using PBF-LB, glasses could be interesting as an electrically insulating material [1-2]. Combing metals and insulating materials allows to build electronic components like sensors and conductors. A concrete future application is a fiber Bragg grating sensor. Using multi-material additive manufacturing, the glass could directly be printed with the structural material which would allow for sensor monitoring of parts [3-4].

The material properties of glasses also lead to challenges in the processing using a laser. A high transmissivity for the commonly used laser wavelength in PBF-LB and a low thermal conductivity compared to metal powders necessitate an optimized strategy for the exposure of glass powders. Additionally, glasses do not have a defined melting point but rather a melting temperature range. The viscosity of the glass strongly depends on the temperature which further complicates the processing since gas cannot escape in the process if the viscosity is too high [5].

The conventional manufacturing of individual parts with complex geometries are either costly, e.g., glass casting or pressing, or time intensive, e. g. laser ablation. The additive manufacturing technologies for which the processability of glasses was already investigated comprise stereolithographic [6], fused deposition modeling [7], ink jet printing [8], and PBF-LB [9-12]. Soda-lime glass is a widely used and cheap material which is suitable for the general studies of glasses. While

recent work for PBF-LB could achieve relative densities as high as 88 % [10], the mechanism and the influence on different scan parameters on the relative density are still not understood completely.

This paper contributes to the understanding of the process parameter of PBF-LB and their influence on the quality of soda-lime glass samples especially on the relative density. As a first step, the raw powder materials were analyzed regarding the flow properties. Afterwards the influence of the laser power, scan velocity, layer height, hatch distance, exposure pattern, preheating, and support structures on the geometrical shape, pore formation and relative density was investigated in different parameter studies.

Nomenclature

Table 1. Description and units of symbols.

Symbol	Description	Unit
h	Hatch distance	mm
P	Laser power	W
s	Layer height	µm
v	Scan velocity	mm/s

Methods and Materials

The experiments with a CO_2-laser were conducted on a DTM Sinterstation 2500 with a laser wavelength of 10.6 µm and a maximum laser power of 67 W. For the fabrication of the soda-lime glass samples with a Yb:YAG laser an EOS EOSINT M270 with a laser wavelength of 1,064 nm and a maximum laser power of 195 W was used. The EOS machine was modified to preheat the platform up to 750 °C. Micrographs of the manufactured glass samples were taken with the light microscope Di-Li 2004 from the company Distelkamp. The powder flowability was analyzed using a Revolution Powder Analyzer. The composition of the soda-lime glass is stated in Table 2.

Table 2. Chemical composition of the soda-lime glass powder according to supplier certificate.

Chemical element	Quantity (wt.-%)
SiO_2	70 to 75
Na_2O	12 to 15
CaO	7 to 12
K_2O	< 1.5
MgO	< 5
Fe_2O_3	< 0.5
Al_2O_3	< 2.5

In Figure 1 the approach for the qualifying of the glass material is illustrated. For the CO_2 laser the approach had to be adjusted to start with single layers as it was technically impossible to expose single tracks. For the Yb:YAG laser single tracks with different parameter sets were built on a aluminum build plate. The results were then transferred for experiments with single and multilayers of the soda-lime glass. Furthermore, the single track width was measured in the microscopy images. The best parameter sets were finally used to build 3-D parts. The influences of the exposure pattern, hatch distance, preheating, and usage of support on the relative density (reference density of 100 %), shape accuracy, and surface quality were investigated further.

Figure 1. Flow chart for the methodical approach for the material qualifying of soda-lime glass by utilizing a Yb:YAG laser.

Results

Powder analysis

The soda-lime powder was investigated with regard to the flowability, particle size distribution (PSD), and sphericity. The rheological properties were measured with two different rotational speeds of 2 and 5 rpm. For each speed three measurements were performed. The resulting rheological properties are listed in Table 3.

Table 3. Measured flowability properties in

Revolutions per minute (1/min)	2	5
Avalanche energy (mJ/kg)	6.23	13.27
Avalanche angle (°)	28.67	30.50
Surface linearity	0.99	0.99

Especially, the avalanche angles of 28.67 and 30.50° indicate a sufficient flowability of the powder and exceed the usual flow properties of metal powders. For comparison, metal powders commonly used in laser-based powder bed fusion show avalanche angles between 30 and 70° [13]. Additionally, the recoating process in the machine with 80, 100, and 200 µm layer thickness showed no groves or other flaws in the powder bed.

To evaluate the sphericity of the powder micrographs were taken. As seen in Figure 2, the powder particles are almost perfectly spherical. A few small satellites can be detected around the glass particles. This is in good correspondence with the measured flow properties, since a spherical particle shape is contributing to high flowability [14].

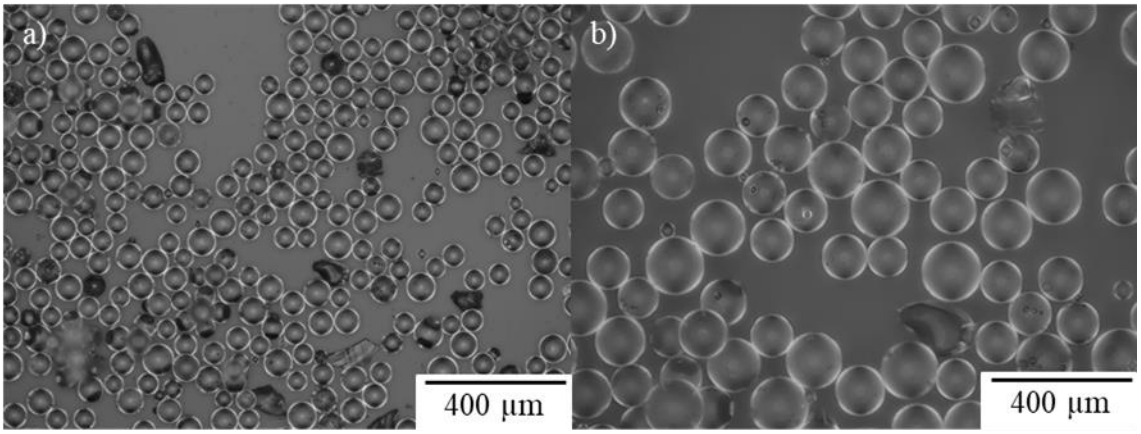

Figure 2. Microscopy images of the soda-lime glass powder with a) 10x magnification and b) 20x magnification.

The average particle size distribution, its standard deviation, as well as maximum and minimum diameter of the particles are stated in table 3. The PSD is narrow (compare Figure 2) and shifted to large particle sizes compared to commonly used metal powders with PSDs between 10 and 100µm [15]. This does not effect the flowability but could lead to a low powder bed density in the process.

Table 3. Particle Size Distribution of the soda-lime glass powder.

Average diameter (µm)	**Standard deviation (µm)**	**Max. diameter (µm)**	**Min. diameter (µm)**
64.95	6.57	79.16	56.9

Investigation of laser applicability for the CO_2 laser

For the limit value observation of the CO_2 laser single layers were built into a loose powder bed. The preparation of single tracks was technically not possible in the corresponding software for the DTM Sinterstation 2500. The single layers seen in Figure 3 were exposed using the maximum laser power of 67 W, the minimum scan velocity of 50.8 mm/s and the minimum hatch distance of 0.08 mm. These parameters yield a maximum area energy density of 16.48 J/mm^2. The number of exposures was varied between one, five, and ten (re-melting).

The single layer built with a tenfold exposure still exhibits holes after the melting. The amount of pores decreases with an increasing number of exposures. Due to this results additional energy input through preheating was tested. A platform heating and radiant heaters were used to increase the powder bed temperature to 160 °C. Due to the elevated temperature, an aluminum build platform was necessary. However, even with preheating the layer was not completely molten and intact particles were visible in the layer. An attempt of recoating and exposing three layers was also not successful. The manual extraction from the build chamber led to a destruction of the parts. Therefore further experiments could not be conducted for the CO_2 laser and the focus was set on the Yb:YAG laser.

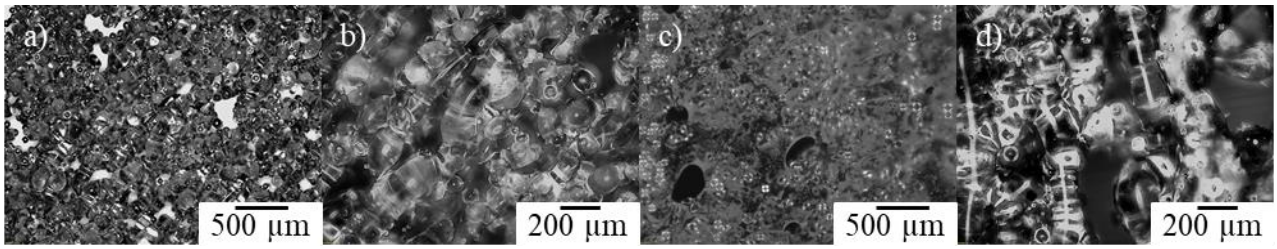

Figure 3. Microscopy images of the soda-lime glass layers exposed with the CO_2 laser. a) one exposure and 10x magnification; b) one exposure and 20x magnification; c) 10x exposure and 10x magnification; d) 10x exposure and 20x magnification.

Single layer single tracks

For the Yb:YAG laser the preparation of single tracks on an aluminum build platform for the first parameter study was possible. The layers for the single tracks were recoated manually and adjusted to values between 0.2, 0.3, 0.5, and 1 mm. The laser power and scan velocity were varied according to Table 4. For layer heights of 0.5 and 1 mm a bonding to the build platform was not possible. The same applied to scan velocities of 100 and 120 mm/s as well as laser powers of 80 and 100 W regardless of the layer height. Furthermore, a laser power of 170 W led to high amounts of spatter, which was therefore excluded in the following experiments.

A parameter combination of scan velocities between 50 to 80 mm/s and laser powers of 120 to 160 W led to complete or at least partial bonding to the build plate for layer heights of 0.2 and 0.3 mm. A further experiment with a layer height of 0.08 mm led to strong balling effects for all parameter combinations. Thus, a layer height of 0.08 mm was not considered for the following studies.

Table 4. Tested parameter combinations and resulting linear energy density for the single tracks with layer heights of 0.2, 0.3, 0.5, and 1 mm.

Scan velocity (mm/s) / **Laser power (W)**	50	60	80	100	120
60	1.20	1.00	0.75	0.60	0.50
80	1.60	1.33	1.00	0.80	0.67
100	2.00	1.67	1.25	1.00	0.83
120	2.40	2.00	1.50	1.20	1.00
140	2.80	2.33	1.75	1.40	1.17
160	3.20	2.67	2.00	1.60	1.33

170	3.40	2.83	2.13	1.70	1.42

Multilayer single tracks

To observe the melting behavior over more than one layer, single tracks with five layers were built. The build platform was preheated to 250 °C to reduce pores and cracks in the specimens. Taking the results of the previous experiment into consideration, layer heights of 0.2 and 0.1 mm were chosen. The top views for the resulting single tracks as well as the varied parameters are summarized in Figures 4 and 5.

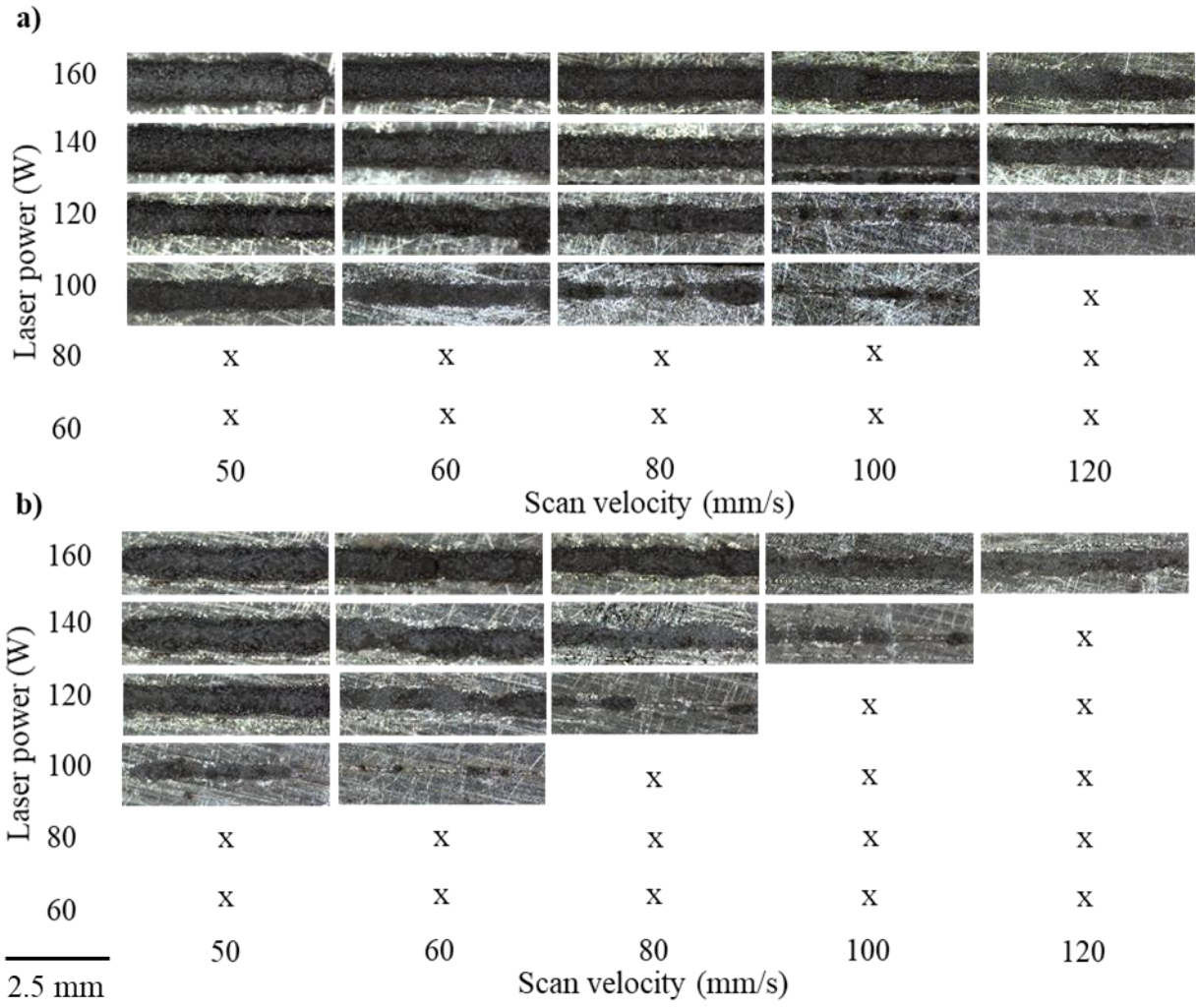

Figure 4. Microscopy images of multilayer single tracks consisting of five layers with a single layer height of 0.1 mm (a) and 0.2 µm (b), built with different parameters. The sections of the single tracks have approximately a length of 5 mm. (x: no material bonded to the substrate).

Neither for a layer height of 0.1 mm nor for 0.2 mm, single tracks were visible after five layers using laser powers of 60 and 80 W. In addition, no material was bonded to the substrate for some single tracks exposed with low energy densities. To evaluate the single tracks, a qualitative scale with the following categories was used: complete and linear single track (full circle), complete single track with necking (empty circle), interrupted single track (triangle), and no visible single track (cross). The qualitative and quantitative results are shown in Figure 4.

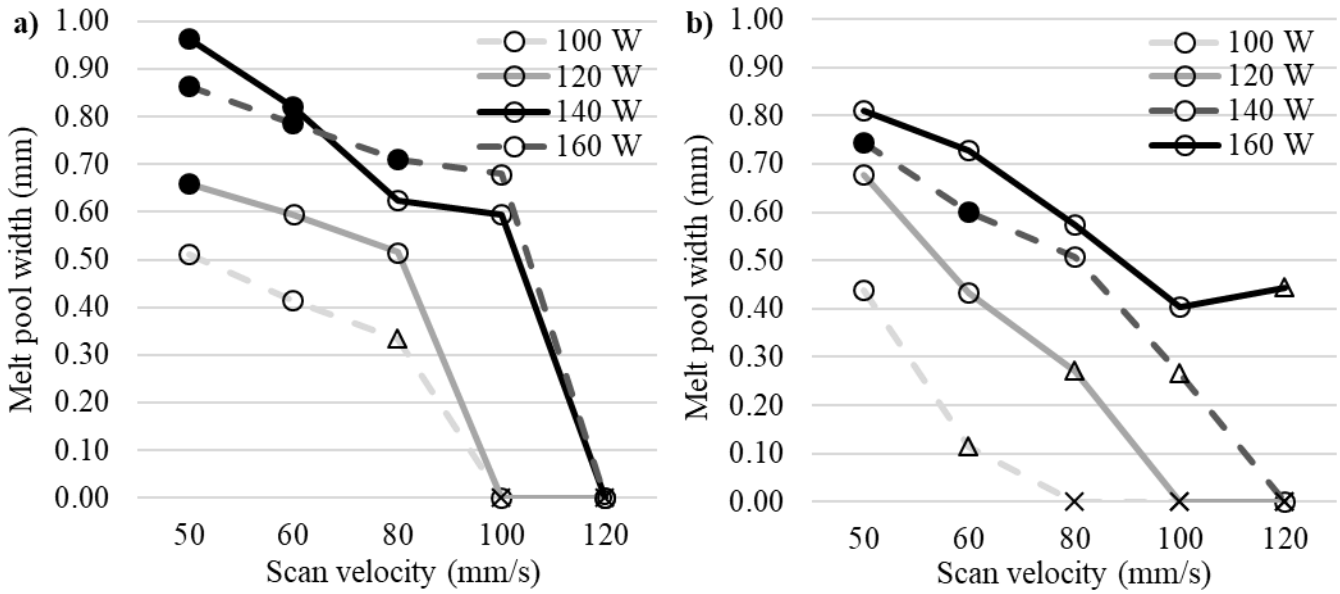

Figure 5. Melt pool width of the multilayer single tracks in dependence of scan velocity and laser power for layer heights of a) 0.1 mm and b) 0.2 mm. Categories: complete and linear single track (full circle), complete single track with necking (empty circle), interrupted single track (triangle), and no visible single track (cross).

Only for linear energy densities higher than 2.4 J/mm the complete single tracks could be bonded to the build plate. For energy densities between 1.5 and 2.4 J/mm, only single tracks with interruptions or necking could be built. Below 1.5 J/mm no material was bonded to the built plate. The melt pool width ranged from 0.4 to 0.96 mm for a layer height of 0.1 mm and from 0.4 to 0.8 mm for 0.2 mm, respectively. Moreover, a positive correlation was found between melt pool width and laser power and a negative correlation for melt pool width and scan velocity. The results show that compared to metals, a higher hatch distance for glasses is necessary due to the large melt pool width.

Single layers

As a next step, single layers were exposed in a loose powder bed with the parameter sets stated in Table 5. The energy density per unit area was varied between 3.75 and 52 J/mm². The aim of the experiment was to gain insight into the melting behavior of a whole layer especially in dependence on the hatch distance. In addition, the exposure into the loose powder bed serves as a rough estimator of the melt pool depth.

Table 5. Tested parameter combinations for the single layers.

Laser power (W)	120, 140 160
Scan velocity (mm/s)	50, 60, 80
Hatch distance (mm)	0.1, 0.2, 0.3, 0.4

In dependence of the energy density the appearance of the resulting layer samples differ significantly. Overall a comparatively high melt pool depth compared to the processing of metals was found. Even with the lowest energy density of 3.75 J/mm² the generated sample had a height of 1 mm. A reason for this could be the high transmissivity of the soda-lime glass powder which is roughly 20 % for a wavelength of 1,064 nm. The laser therefore penetrates deep into the powder bed resulting in high melt pool depths. Notable is the strong proneness to spherical sample shapes for high energy densities. In Figure 6 three samples are shown in top and side view. The samples in Figure 6 a) and b) have a round shape which results from long solidification time and large melt pools. The soda-lime glass has a lower thermal conductivity than metals, which is further reduced due to the powder bed. The melt has the tendency to build spherical droplets to reduce the surface area. In common PBF-LB processes the

material, especially metals, solidifies rapidly which prohibits this tendency. This spherical shape is observed for all energy densities higher than 17.5 J/mm². For energy densities between 8 and 17.5 J/mm², a nearly quadratic area occurs. Below 8 J/mm² the particles were only partly sintered and therefore no connected sample could be manufactured.

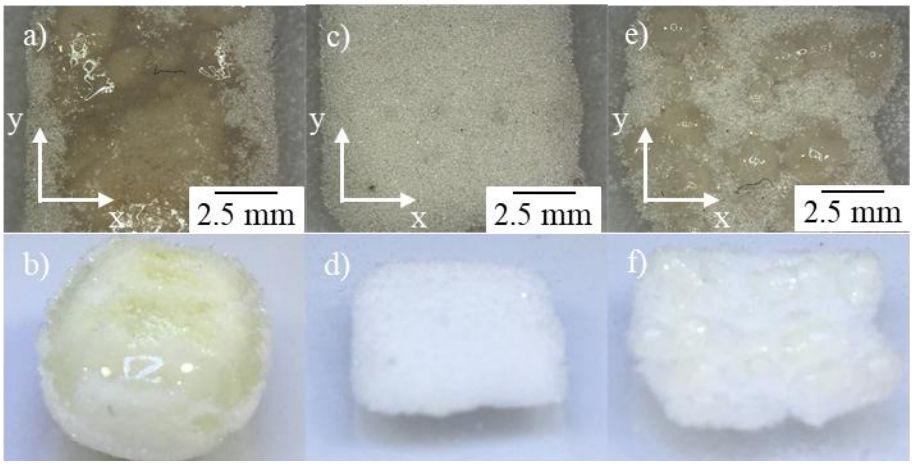

Figure 6. Images of multilayer single layers exposed into a lose powder bed (build-direction: z-axis, isometric view in the bottom images). a) and b) P = 140 W, v = 50 mm/s, h = 0.1 mm; c) and d) P = 160 W, v = 80 mm/s, h = 0.2 mm; e) and f) P = 160 W, v = 50 mm/s, h = 0.3 mm.

Multilayers

Based on the results of the single layer and single tracks experiments a parameter study for small 3-D parts was designed. Cuboid shaped samples with dimensions of 3 x 20 x 3 mm^3 (width x length x height) were built. The samples depicted in Figure 7 have a curvature in the middle regardless of the scan parameters. This phenomena has the same cause as the aforementioned spherical shape for the single layers. For high energy densities this curvature led to the tearing off of the samples from the aluminum build plate.

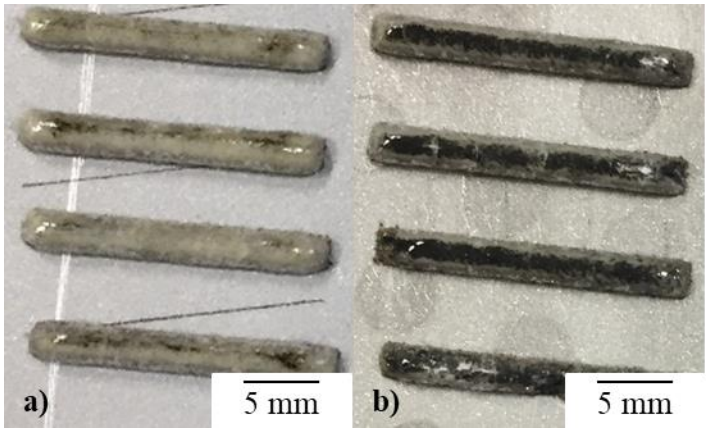

Figure 7. Pictures of the cuboid samples with layer heights of a) 0.2 mm and b) 0.1 mm.

The three microscopy image in Figure 8 show the tendency of pore formation for low energy densities. In Figure 8 c) an increased number of pores was observable around the middle of the sample. With increasing energy density the pores were reduced. This trend is dependent on which scan parameter was adjusted. A decreasing layer height (see Figure 8 a) or hatch distance as well as a decreasing scan velocity (see Figure 8 b) led to a reduced amount of pores while an increase in laser power from 140 to 160 W did not affect the number of pores. The cause of the strong pore formation for the soda-lime glass is the low viscosity of its melt. Some elements of the glass powder evaporate

through the heat. The melt solidifies before the gas can escape. Also noticeable are the sintered particles at the sample edges.

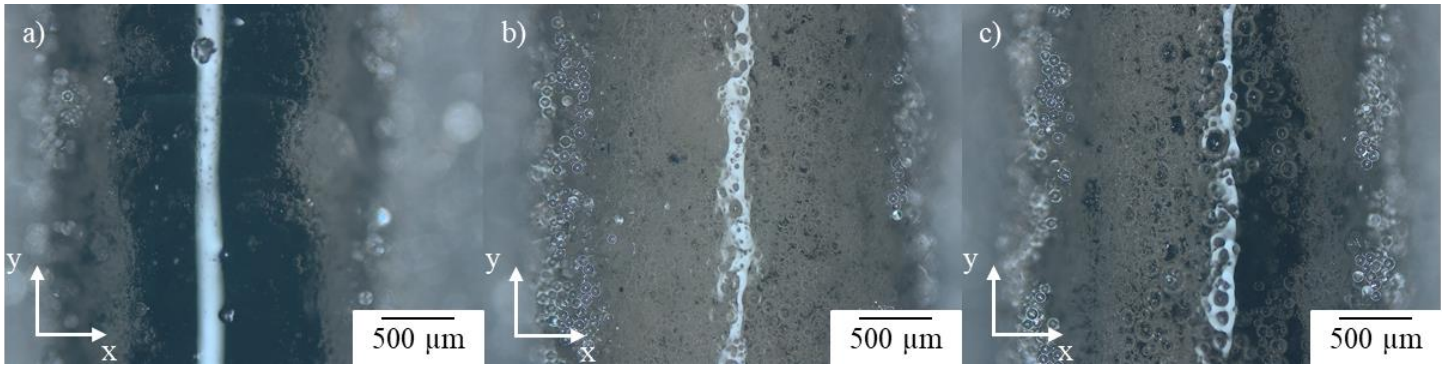

Figure 8. Pore formation in soda-lime glass samples. Build parameters: P = 160 W; a) s = 0.1 mm, h = 0.3 mm, v = 66 mm/s; b) s = 0.2 mm, h = 0.3 mm, v = 66 mm/s, c) s = 0.2 mm, h = 0.03 m, v = 52 mm/s.

3-D parts

For the manufacturing of cubes with an edge length of 10 mm, the previous results were taken into account. The parameter sets used for the first cubes are displayed in Table 6. As the curvature in the previous experiments was more pronounced in the samples built with a layer height of 0.1 mm, a layer height of 0.2 mm was chosen for all following samples. All parameter combinations were exposed with a line pattern and a preheating of 250 °C was used.

Table 6. Variation of laser power, scan velocity and hatch distance for the 10 x 10 x 10 mm³ cubes (x: sample not successfully built).

Laser power (W)	Scan velocity (mm/s)	Hatch distance (mm)	VED (J/mm³)	Relative density (%)
140	50	0.2	70	x
		0.3	46.7	81.7
		0.4	35	74.6
	60	0.2	58.3	x
		0.3	69.2	77.7
		0.4	29.2	69.2
		0.5	23.3	68.5
160	50	0.2	80	x
		0.3	53.3	x
		0.4	40	x
		0.5	32	80.1
	60	0.2	66.7	x
		0.3	44.4	x
		0.4	33.3	82.1
		0.5	26.7	x
	80	0.2	50	x
		0.3	33.3	82.2
		0.4	25	x
		0.5	20	x

For hatch distances of 0.2 mm the samples could not be successfully built due to their high curvature in the middle of the sample. At the same time a strong spatter formation was observed. As a

tendency, volumetric energy density higher than 46.7 J/mm³ led to an abortion of the respective samples. The only exception is the sample built with a laser power of 140 W, a scan velocity of 60 mm/s and a hatch distance of 0.3 mm. Furthermore, a volumetric energy density of around 30 J/m³ led to good result in terms of relative density with the highest achieved relative density being 82.2 %.

Influence of build parameters on the relative density

As a further investigation, chess board exposure pattern was tested in comparison with line board exposure pattern. The samples built with chess board exposure pattern showed less curvatures. In Figure 9 the images of samples exposed with line and chess board pattern are depicted. No effect on the overall relative density can be observed when comparing the exposure patterns but the pores are distributed more evenly over the cross-section of the samples. A possible reason for this could be the more equally distributed heat using a chess board pattern, which leads to smaller but at the same time to a higher amount of pores.

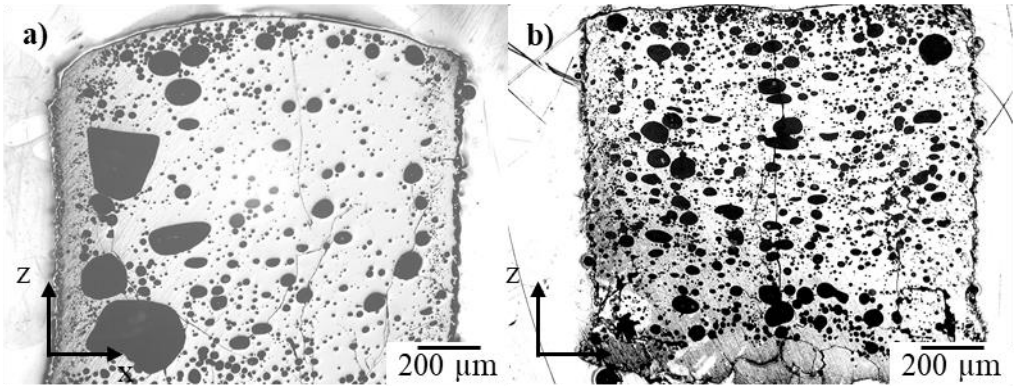

Figure 9. Comparison of the curvature of samples exposed with (a) line and (b) chess board pattern. P = 140 W, v = 50 mm/s, s = 0.2 mm, h = 0.3 mm

Furthermore, a higher preheating temperature led to a decrease of the thermally induced stresses due to lower temperature differences between the melt and the solidified areas [16]. Therefore, the influence of the preheating temperature on the relative density was investigated. Thus, the platform heating was varied between 250, 550, and 600 °C. The achieved relative densities for different scan parameters in dependence on the platform heating are shown in Figure 10.

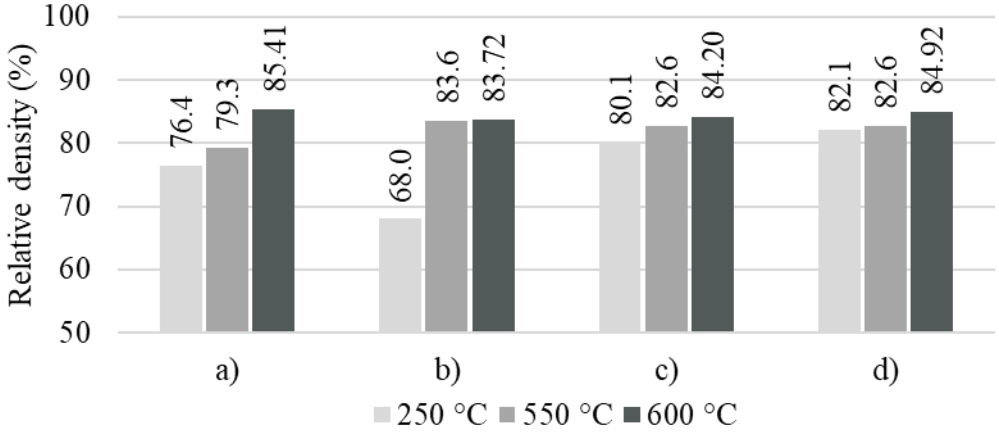

Figure 10. Relative density of cubes built with different preheating temperatures a) P = 140 W, v = 50 mm/s, h = 0.4 mm; b) P = 140 W, v = 60 mm/s, h = 0.4 mm; c) P = 160 W, v = 50 mm/s, h = 0.5 mm; d) P = 140 W, v = 80 mm/s, h = 0.5 mm.

For the four parameter combinations an increase of the relative density with increasing preheating temperature was achieved. In Figure 11 three different samples built with different preheating temperatures are illustrated. The viscosity of the glass decreased for higher temperatures, which facilitates the escaping of the gas from the melt. In average, this led to smaller pore sizes in the samples with higher preheating temperatures. Additionally, the cube in Figure 11 a) shows a large crack in the middle and a few more originating from the large crack itself. As the low preheating led to high temperature differences between the currently melted regions to the solidified regions thermal stresses were induced. These stresses can be minimized by a sufficient preheating. Figure 11 b) and c) show samples which were built with preheating temperatures of 550 and 600 °C, respectively. Nearly no cracks are seen in these samples. The crack in Figure 11 c) probably resulted from thermal stresses induced by temperature differences of the build plate and the sample. Moreover, comparatively large pores can be found at the bottom of the samples near the build plate. The pronounced pore formation could be attributed to evaporated aluminum of the build platform.

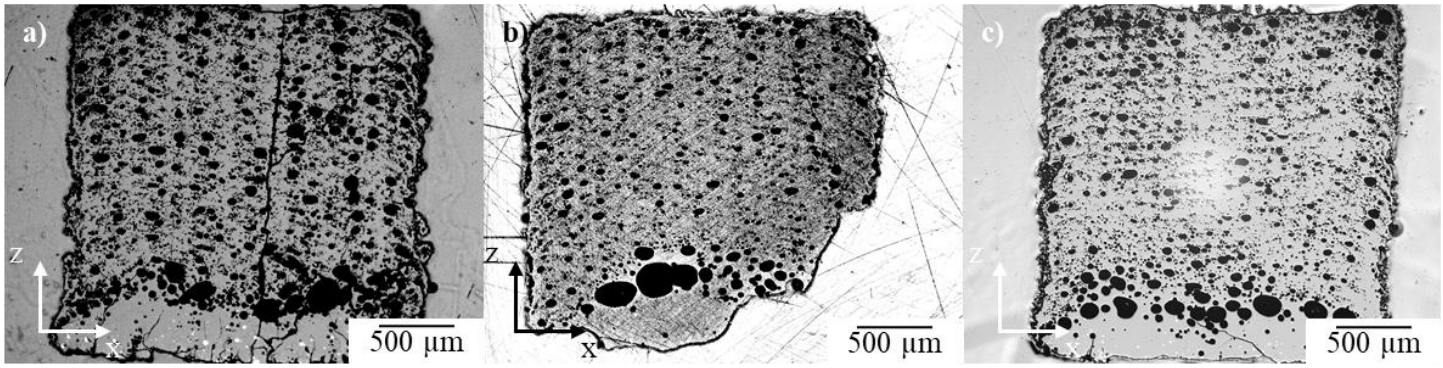

Figure 11. Comparison of samples built with different preheating temperatures a) 250 °C, b) 550 °C (part of the sample broke off during the extraction), and c) 600 °C. Other parameters: P = 160 W; v = 50 mm/s; h = 0.5 mm.

Test samples with support structures were built and compared to samples without support. The support was built separately before and in a second built process the samples were built on it. In Figure 12 a) a sample with a support structure is depicted. Missing pores at the bottom of the sample in vicinity of the build plate are noteworthy. The cause is probably that the aluminum build plate does not evaporate as the distance from the first exposure is higher. Remarkable is the low porosity in the support structure (marked in red) which is also fused together by the two step process. The low porosity cannot be explained conclusively. Furthermore, the sample built with support structure also shows a strong deviation in the height. With a height of 13.47 mm the sample is 3.47 mm higher than it should be according to the prepared data.

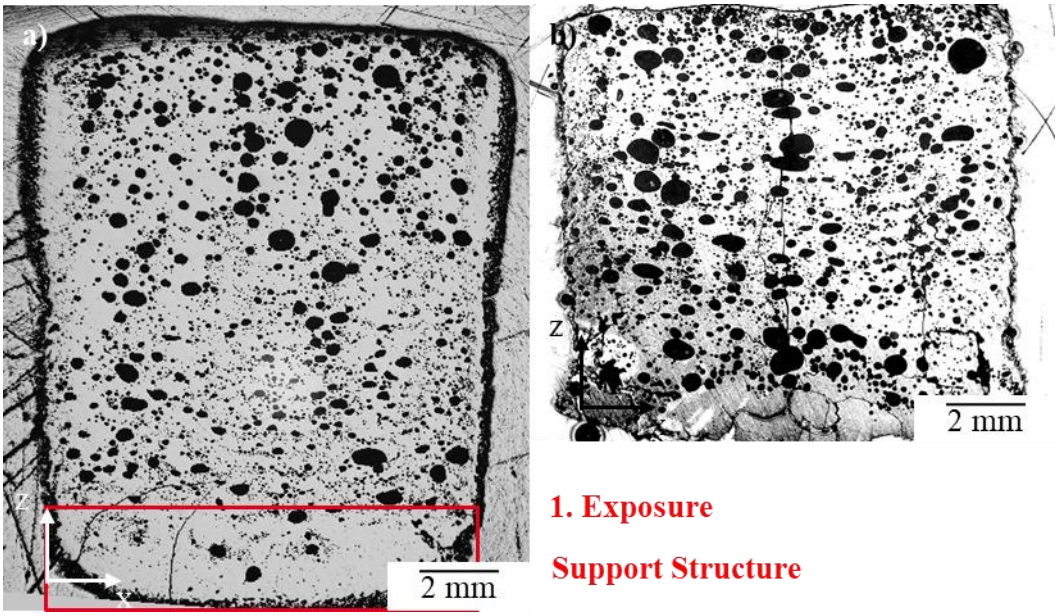

Figure 12. Comparison of cubes built with a) and without support structure b). The marked red area shows the support below the sample.

The diagram in Figure 13 shows that only a small increase in relative density could be achieved for the samples with a support structure. The highest achieved relative density of 88.7 % was manufactured with support structure and scan parameters of 140 W laser power, 50 mm/s scan velocity, 0.3 mm hatch distance, 0.2 mm layer height, and a line pattern.

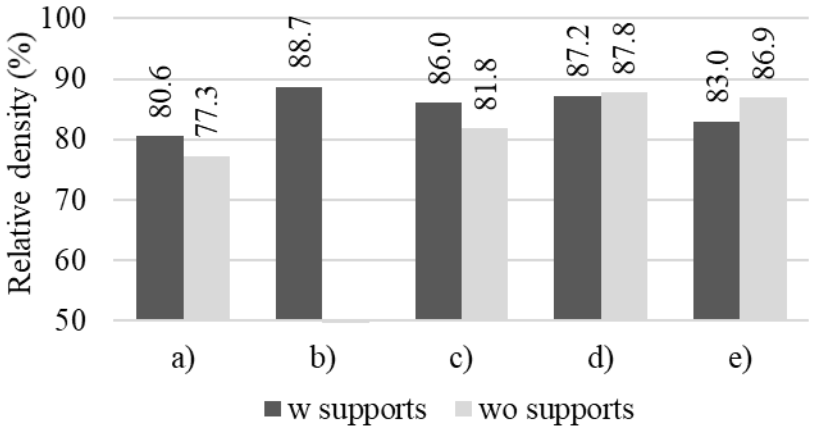

Figure 13. Comparison of the relative density of cubes built with (w) and without (wo) support structures. Laser power for all samples 140 W. a) v = 60 mm/s, h = 0.3 mm, LP; b) v = 50/mm/s, h = 0.2 mm, CB; c) v = 50 mm/s, h = 0.3 mm, CB; d) v = 60 mm/s, h = 0.2 mm, CB; e) v = 60 mm/s; h = 0.3 mm, CB

Conclusion and Outlook

This paper presented an approach to develop parameters for the processability of soda-lime glass in PBF-LB. Looking at the most important build parameters laser wavelength, laser power, scan velocity, layer height and hatch distance, the key findings can be summarized as follows:

- The manufacturing of 3-D-parts using soda-lime glass in PBF-LB is generally possible.
- A relative density of 88.7 % was achieved.
- A CO_2-laser with the respective laser power of 67 W is not sufficient to melt complete and continuous layers.
- A strong tendency of gas porosity due to the high viscosity of glass was observed.

The found interrelations and dependencies differ extensively from the processing of metals in PBF-LB. Notable points regarding the preheating, support structures and exposure patterns are:

- Preheating of the platform led to reduced pore formation and therefore higher relative densities.
- Support structures did not affect the relative density of soda-lime glass parts.
- Chess board exposure patterns reduced the curvature of the samples but did not increase the relative density.

There a different outstanding aspects which should be addresses in future research. Especially a more detailed look into the physics of the process and further adaptions of the standard PBF-LB process are important:

- A compensation strategy for the long solidification time, e. g.by extending the waiting time between neighboring laser vectors.
- For a better understanding of the pore formation and the general process, the use of a high speed camera system could allow deeper insights.
- In terms of multi-material fabrication the bonding of glass to metals or other material classes should be examined.

Acknowledgements

The authors express their sincere thanks to the State of Bavaria and its Bavarian Ministry of Economic Affairs, Regional Development and Energy StMWi for funding the "MULTIMATERIAL-Zentrum Augsburg". Furthermore, the authors thank Paul Rob for the execution of the specimen analysis within his master thesis.

Literature

[1] M. Binder, M. Fischer, S. Dietrich, C. Seidel, G. Reinhart (2020). Integration of Strain Gauges in Components Manufactured by Laser-Based Powder Bed Fusion, MIC Procedia 034–04.

[2] M. Binder, L. Kirchbichler, C. Seidel, C. Anstätt, G. Schlick, G. Reinart (2019). Design Concepts for the Integration of Electronic Components into Metal Laser-based Powder Bed Fusion Parts. In: Procedia CIRP 81, S. 992–997.

[3] J. Mathew, D. Havermann, D. Polyzos, W. N. MacPherson, D. P. Hand, R. R. J. Maier, SS316 structure fabricated by selective laser melting and integrated with strain isolated optical fiber high temperature sensor. In: Hypolito J. Kalinowski, José Luís Fabris und Wojtek J. Bock (2015.): 24th International Conference on Optical Fibre Sensors. Curitiba, Brazil: SPIE Proceedings, 96340Q.

[4] D. Havermann, J. Mathew, W. N. MacPherson, R. R. J. Maier, D. P. Hand (2015). Temperature and Strain Measurements With Fiber Bragg Gratings Embedded in Stainless Steel 316. In: J. Lightwave Technol. 33 (12), S. 2474–2479.

[5] H. Shang, T. Rouxel (2005). Creep Behavior of Soda-Lime Glass in the 100–500 K Temperature Range by Indentation Creep Test, Journal of the American Ceramic Society,Volume 88 (9), 2625-2628.

[6] Kotz, K. Arnold, W. Bauer, D. Schild, N. Keller, K. Sachsenheimer, T.M. Nargang, C. Richter, D. Helmer, B.E. Rapp (2017). Three-dimensional printing of transparent fused silica glass, Nature vol. 544 (7650) 337–339.

[7] D.T. Nguyen, C. Meyers, T.D. Yee, N.A. Dudukovic, J.F. Destino, C. Zhu, E.B. Duoss, T.F. Baumann, T. Suratwala, J.E. Smay, R. Dylla-Spears (2017). 3D-printed transparent glass, Adv. Mater. 29 (26) 1–5.

[8] J.F. Destino, N.A. Dudukovic, M.A. Johnson, D.T. Nguyen, T.D. Yee, G.C. Egan, A., M. Sawvel, W.A. Steele, T.F. Baumann, E.B. Duoss, T. Suratwala, R. Dylla-Spears, 3D printed

optical quality silica and silica – titania glasses from sol – gel feedstocks, Adv. Mater. Technol. 3 (1700323) (2018) 1–10.
[9] K.C. Datsiou, E. Saleh, F. Spirrett, R. Goodridge, I. Ashcroft, D. Eustice (2019). Additive manufacturing of glass with laser powder bed fusion, J. Am. Ceram. Soc. 102, 4410–4414.
[10] K.C. Datsiou, F. Spirrett, I. Ashcroft, M. Magallanes, S. Christie, R. Goodridge (2021). Laser powder bed fusion of soda lime silica glass: Optimisation of processing parameters and evaluation of part properties
[11] M. Fateri, A. Gebhardt (2015). Selective laser melting of soda-lime glass powder, Int. J. Appl. Ceram. Technol. 12 (1), 53–61.
[12] M. Fateri, A. Gebhardt, S. Thuemmler, L. Thurn. (2014). Experimental investigation on selective laser melting of glass. *Physics Procedia, 56*, 357–364.
[13] Spierings, M. Voegtlin, T. Bauer, K.Wegener (2016). Powder flowability characterisation methodology for powder-bed-based metal additive manufacturing in Progress in Additive Manufacturing volume 1, 9–20
[14] S. E. Brikaa, M. Letenneura, C. A. Dion, V.Brailovskia (2020). Influence of particle morphology and size distribution on the powder flowability and laser powder bed fusion manufacturability of Ti-6Al-4V alloy, Additive Manufacturing, Volume 31, 100929.
[15] K. G. Prashanth, (2018). Influence of Powder Characteristics on Processability of AlSi12 Alloy Fabricated by Selective Laser Melting. In: Materials (Basel, Switzerland) 11 (5).
[16] K. Kempen, B. Vrancken, S. Buls, L. Thijs, J. van Humbeeck, J.-P. Kruth (2014). Selective Laser Melting of Crack-Free High Density M2 High Speed Steel Parts by Baseplate Preheating, *J. Manuf. Sci. Eng*., 136(6): 061026